Physics of the Solid State, 2023, Vol. 65, No. 6

02,13

Oxygen distribution in the structure of $YBa_2Cu_3O_{7-\delta}$ thin films after vacuum exposure at 300 K

© A.I. Il'in[1], A.A. Ivanov[2], V.K. Egorov[1]

[1] Institute of Microelectronics Technology and High Purity Materials, Russian Academy of Sciences, Chernogolovka, Russia
[2] National Research Nuclear University „MEPhI",
Moscow, Russia

E-mail: alivil2017@yandex.ru

Received April 17, 2023
Revised April 17, 2023
Accepted May 11, 2023

We have found out that vacuum exposure of $YBa_2Cu_3O_{7-\delta}$ thin epitaxial films at 300 K for 24 hours decreases oxygen content and induces changes in their crystal structure depending on the films synthesis conditions. $YBa_2Cu_3O_{7-\delta}$ films on $SrTiO_3$ (100) substrates were synthesized by pulsed laser deposition. The crystal structure was studied using XRD technique. Additional maxima of diffraction peak (005) before and after vacuum exposure indicate the presence of regions with different oxygen content; and the change in the shape of the rocking curves indicate a change in the crystallites orientation. After vacuum exposure, the oxygen deficiency δ in the films increased from ~ 0.01 to ~ 0.6 for films with a crystallites size of 2−10 nm and from $\sim 0.25-0.35$ to ~ 0.6 for crystallites size of 500−1000 nm. The appearance of a residual resistance after the superconducting transition in the dependence R(T) may be explained by the fact that oxygen loss mainly in the boundary regions of the crystallites takes place, so that their boundaries become dielectric, while the crystallites themselves remain superconductive. Based on the data of X-ray diffraction analysis, as well as resistive measurements, we have come to the conclusion about oxygen loss through grain boundaries in films with nanocrystallites of 2−10 nm in size, and also through structural defects in films with larger crystallites.

Keywords: pulsed laser deposition, surface relief, transport characteristics of films, film evolution, $SrTiO_3$.

DOI: 10.21883/PSS.2023.06.56094.28H

1. Introduction

Superconducting properties of thin $YBa_2Cu_3O_{7-\delta}$ (YBCO) films depend on the oxygen content, which may be measured by X-ray diffraction analysis methods, by resistance/temperature dependence $R(T)$ in plane 'ab', by positron annihilation spectroscopy with variable positron beam [1–8]. Thin films with optimum content of oxygen corresponding to index $y = 7 - \delta \sim 6.85$ and equilibrium homogeneous structure have superconducting (SC) transition end temperature $T(R = 0) = 85-90$ K [1,5,6,9–13] with $R(T)$ in the normal state being proportional to the temperature. $R(T)$ values are defined by resistance of CuO_2 planes, because resistance at 300 K of a single CuO_2 plane is almost independent on the chemical composition of cuprates [1,5]. When oxygen content is lower than the optimum value, linear section of $R(T)$ in YBCO films is reduced and forms a concave curve with decreasing temperature. A higher oxygen deficiency changes $R(T)$ to a parabolic convex curve due to partial removal of the dominating scattering channel [1,2,14,15]. Loss of superconducting properties of films correspond to oxygen deficiency $\delta \sim 0.7$ and higher. The optimum content of oxygen obtained during deposition is maintained in films or film-based 2D devices by provision of a buffer layer on the free surface [14]. When films without the buffer layer are held at 10^{-3} Pa, T_c is reduced, SC transition width and oxygen content δ increase [12]. M. Reiner *et al.* [7] found that loss of oxygen by 230 nm films starts at a temperature a little higher than 240°C. The nature and mechanism of loss of oxygen were not defined. The YBCO film produced by laser deposition followed by annealing in 400 mbar oxygen at 400°C, oxygen deficiency δ decreased from 0 on the free surface to 0.4 at the boundary of the film−substrate interface [7]. After vacuum exposure, δ varied from 1.05 on the free surface to 0.25 at the substrate. Moreover, positron beam scanning allowed to detect spatial variation δ that appeared to vary with a standard deviation up to 0.079 from the mean value within a YBCO film [8]. Comparative analysis of X-ray diffraction data, morphology and resistance/temperature dependence $R(T)$ of films allowed to correlate the loss of oxygen in thin YBCO films deposited at a rate lower than 0.1 nm/s with formation and growth of oxygen-depleted pyramids. Taking into account the growth of spiral pyramids above the surface profile, oxygen diffusion path on spiral pyramid defects along their heights was suggested [15,13]. Height of such pyramids [2,5,11,15–17] achieved 80 nm or 30% of the film thickness, which was much higher than 5 nm high irregularities in 10−50 nm films [14] at minimum free surface roughness near 1.1 nm — lattice constant along the crystallographic axis c.

Comparative analysis of X-ray diffraction and resistance properties of films before and after vacuum exposure during 24 h at 300 K was carried out herein for YBCO films produced in various deposition conditions. The findings show loss of oxygen after vacuum exposure of films with $2-10$ nm crystallites to $\delta \sim 0.5$ and of films with large pyramids of ~ 500 nm to ~ 0.3. Oxygen content variation was followed by crystallite reorientation in films. Structure-induced loss of oxygen in more desirable in terms of electrophysical properties YBCO films suggested oxygen diffusion paths, which is almost necessary knowledge for the development of pulsed laser deposition techniques [14,17] and creation of nanotechnologies to investigate physical phenomena and produce 2D instruments and devices [17–21].

2. Experimental

YBCO films were synthesized by pulsed laser deposition(PLD) on $SrTiO_3(100)$ single-crystal wafers with surface roughness range up to 2 nm and rms deviation of roughness $Rq = 0.14$ nm. Before deposition, 5×10 mm and 0.5 mm thick wafers were etched in $(H_2SO_4 + HNO_3)$ mixture and washed in distilled water. Films with a thickness of $150-200$ nm were produced using velocity filtration technique, while films with a thickness of 300 nm were produced without filtration (Table). The PLD unit, detailed in [13,15–17], consisted of CL7100 excimer laser (wavelength 248 nm, pulse length 15 ns), WPP-4 upgraded vacuum setup equipped with a Varian SH-110 pump and Varian TPS-compact turbomolecular system. This setup was designed to achieve oil-free vacuum in the evaporation chamber and to vary the oxidizing medium pressure from 1 atm to 10^{-6} Torr. Pulse repetition rate of the material deposited to the substrate (filtering frequency N) was set by the laser ignition synchronization system with window positions in the disk and, for the purpose of our experiments, was equal to the laser pulse frequency. The laser pulse frequency limit for deposition was lower than the disk rotational frequency (n), which was changed from 90 to 160 Hz, therefore, a frequency divider was used for laser ignition, so n/N in different experiments was from 5 to 20. The minimum velocity of the particles passing through a disc window, hereinafter referred to as cut-off velocity, is $V_0 = L/T$, where the disk distance from the target is $L = 30-35$ mm, and $T = d/(2\pi \cdot D \cdot n)$; where$D$ is the distance between the hole center and the axis of disc rotation (75 mm), and d is the diameter of this hole. Film thickness was measured using Dektak-150 stylus profiler. Surface morphology was examined in EVO-50 SEM. $R(T)$ of the films was measured on 5×10 mm chips using a four-probe method. Contacts in the form of four 0.5 mm wide silver strips were deposited on a YBCO film across the long side of the chip with inner potential stripes spaced at 7 mm. The following values were determined on $R(T)$ for each sample: R_{92} — resistance in normal state before SC transition, $T(R = 0.9R_{92})$, $T(R = 0.1R_{92})$ — transition temperatures at 0.9 and 0.1 from R_{92}, respectively, $\Delta T = T(R = 0.9R_{92}) - T(R = 0.1R_{92})$, $T(R = 0)$ — transition end temperature. X-ray diffraction study was carried out using HZG-4 diffractometer with a fixed anode and BSV-28 tube($CuK_\alpha = 1.54178$ Å) at 20 kV and 22 mA in the focusing Bragg–Brentano $\theta-2\theta$ [22] geometry with a radius of $R = 235$ mm. The initial X-ray beam was formed by a vertical slit 0.1 mm in width and 10 mm in height as well as by a horizontal Soller slit with a wafer-to-wafer distance of 1 mm. With X-ray source focal width 1.0 mm, sampling angle 6° and distance from the focal spot to the cut-off slit of 50 mm, a beam with horizontal divergence $\Delta\varphi = 0.2°$ was formed. The vertical divergence determined using the Soller slit was 2°. However, the use of the Soller slit in front of the detector slit made it possible to reduce the angular divergence in the recorded reflections to $\Delta\psi = 0.2°$. The diffraction pattern was recorded by a scintillation detector with a cur-off slit 0.1 mm in width and 10 mm in height. The diffraction data was collected in the step-by-step scanning mode with the recording step for each measurement from 0.01 to 0.005° within 10 s. Energy discrimination of the recorded diffraction lines was performed with „Ortec“ SCA-550 type single-channel analyzer. In this case, the contribution of the „white“ component to the intensity of the recorded diffraction lines did not exceed 5%. Oxygen content in the films was calculated from precision measurements of the angular position of the maximum reflection (005) [6]. Orientation of the single-crystal film grains was determined using the so-called rocking curves [23] representing the angular dependence of the intensity in the diffraction peak (005) of YBCO ($2\theta_{005} \sim 38.1°$) with the counter fixed in the maximum intensity position.

After completion of the X-ray diffraction analysis and determination of $R(T)$, the deposited films were held in 10^{-6} Pa 24 h vacuum at 300 K, and then the measurements were repeated. For 300 nm film 7, the illustrated X-ray diffraction peak intensities were recalculated to the mean thickness of other films 175 nm (with coefficient (arb. units/$300 \cdot 175$)).

3. Results

3.1. Measurements of $R(T)$ of films

Film samples $1-2$, $3-4$, $5-6$ with a thickness of $150-200$ nm deposited in different conditions using velocity filtration technique had $T(R = 0) = 85-85.8$, 84, 77.4 K, and 300 nm sample 7 was deposited without velocity filtration and had $T(R = 0) = 87$ K (see the Table). After deposition, dependences $R(T)/R_{300}$ (where R_{300} is the film resistance at 300 K) were typical for the films with an oxygen index of at least $y = 6.5$ [1,9–12,24,25] (Figure 1), i. e. were linear on the most part of the temperature range from 300 K to the SC transition, but had different $T(R = 0)$, $T(R = 0.9R_{92})$, $T(R = 0.1R_{92})$, ΔT depending on the velocity filtration and deposition

Deposition conditions, structure and SC transition characteristics before and after vacuum exposure*

Film №	d, mm	V_0, 10^4 m/s	N, Hz	Å/s	T, K ($0.1R_{92}$)	T, K ($0.9R_{92}$)	ΔT, K	$T(R=0)$, K K	δ	FWHM, (005) deg.**	FWHM, (005) deg.***
1	10	2.0	28	4.9	89.2 (82.2)	86.4 (–)	2.8 (–)	85 (–)	0.12 (0.59)	– (0.16)	0.9 (0.33)
2	10	2.3	33	5.8	90.5	88	2.5	85.8	0.09 (0.58)	0.21 (0.32)	– (0.79)
3	10	1.5	21	6.2	90 (84.1)	86.6 (–)	3.4 (–)	84 (–)	0.17 (0.18)	0.2 (0.21)	– (0.365)
4	8	1.9	21	6.1	90.2	87.6	2.6	84	0.07 (0.16)	0.14 (0.18)	0.7 (0.64)
5	6	2.1	4.5	0.5	82	< 77.4	–	< 77.4	0.24 (0.62)	– (0.14)	0.58 (0.69)
6	6	3.0	6.5	1.1	84 (80)	80.5 (–)	3.5 (–)	77.4 (–)	0.35 (0.6)	0.115 (0.19)	– (0.55)
7	–	–	15	4.5	90.8 (88.4)	88.4 (–)	2.4 (–)	87 (–)	0.08 (0.45)	0.15 (0.15)	0.58 (0.7)

Note. * Characteristics of films without brackets were obtained after deposition, and in brackets — after storage in vacuum 10^{-6} Ra 24 h. ** results of FWHM determination on the angular dependence of intensity (005) in the focusing geometry Bragg–Brentano $\theta-2\theta$ [22], *** results of FWHM determination from rocking curves [23] representing the angular dependence of intensity (005).

conditions (see the Table). Values R_{300} decreased (Table in Figure 1) with decreasing filtering frequency (see the Table) both before and after vacuum exposure. Films with a thickness of 300 nm deposited without velocity filtration had the lowest R_{300}, high $T(R=0)=87$ K, narrow SC transition with $\Delta T = 2.4$ K and oxygen deficiency estimated by C-parameter $\delta = 0.08$ (see the Table). Vacuum exposure increased the resistance at 300 K in films 1, 3, 6 and 7 in such a way that R_{vac}/R_{dep} (where R_{dep} and R_{vac} are prior and post vac film resistances) was equal to ~ 130, 22, 25 and 18, respectively.

High-temperature linear section of $R(T)/R_{300}$ became convex in post vac films 1, 6 and concave in film 3 suggesting higher oxygen content in the conducting volumes of this film than in films 1 and 6 (Figure 1) [12]. This comparison is also supported by the X-ray diffraction analysis, where oxygen deficiency $\delta = 0.18$ averaged by the volume of film 3 was lower $\delta = 0.6$ in films 1 and 6 (see the Table). The maximum rise of δ occurred in films 1 and 2 deposited from particles up to 40 nm at a filtratin frequency of 28–33 Hz [15]. Since oxygen is the most mobile element among all elements in the film, then increase in R_{dep}/R_{vac} by a factor more than 18 after vacuum exposure at 300 K could be obtained only by varying its amount and/or distribution in the film structure. $T(R=0.9R_{92})$ after vacuum exposure of films 1, 3, 6 and 7 decreased by 7, 6, 4, 2.5 K, respectively. Variation of the high-temperature section shape of $R(T)/R_{300}$ of post vac films may be associated both with reduction of scattering centers that define $R(T)$ slope before vacuum exposure and with the impact o boundaries that will provide growing contribution to the resistance with

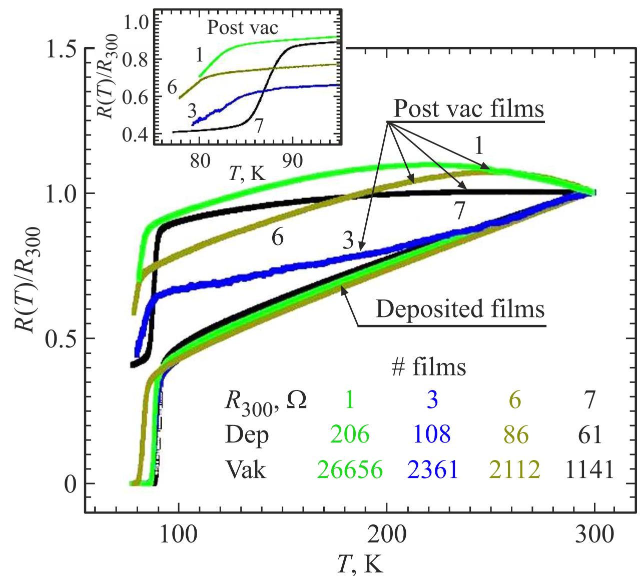

Figure 1. $R(T)/R_{300}$ of films with different T $(R=0)$: *1* — 86; *3* — 84; *6* — 78; *7* — 87 K. The Table shows R_{300} of prior and post vac films. The inset shows the zoomed-in view of SC transition of post vac films.

decreasing temperature. However, the prevailing reduction of $R(T)/R_{300}$ with decreasing temperature may suggest that resistances of CuO_2 planes have prevailing impact on the total resistance, rather than grain boundaries. Almost linear and more level section (compared with the deposited film) of $R(T)/R_{300}$ in the normal state of post vac film 7 suggested the reduction of resistance scattering centers

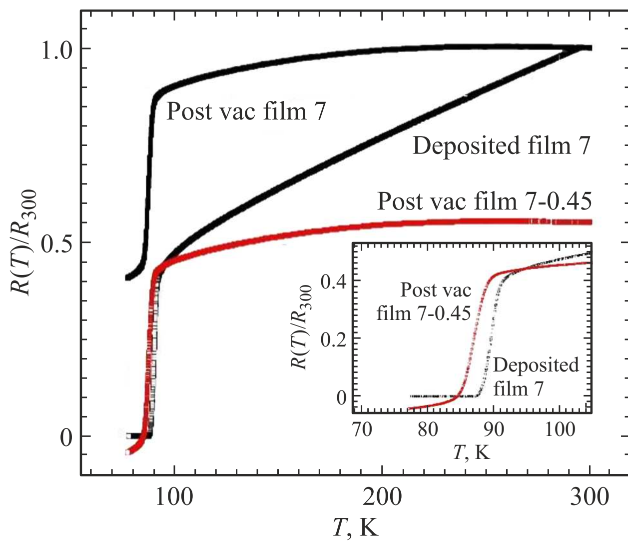

Figure 2. $R(T)/R_{300}$ of prior and post vac film *1* with $T(R=0) = 87$ K (for comparison of the SC transitions, post vac curve $R(T)/R_{300}$ is shifted down by 0.45 and highlighted in red). The inset shows the zoomed-in view of the SC transition region.

(Figure 2). Oxygen atoms whose number decreased by $\Delta\delta = 0.37$ may be the most probable centers. With SC transition generally maintained after vacuum exposure, it ended at ~ 77.2 K and residual resistance $\sim 57\,\Omega$. Residual resistance is also present in films 1, 3, 6, since $R(T)/R_{300}$ before SC transition in them increased by 0.25–0.45 after storing in vacuum. The presence of residual resistance in all films proves that additional resistance occurs in CuO_2 (00l) planes after vacuum exposure.

3.2. XRD study in $\theta - 2\theta$ geometry

Peak intensity (005) in films deposited with velocity filtration was higher with decreasing filtration frequency. After vacuum exposure, reflection intensities in films 2, 3, 6 decreased by 23–100%, and in increased by 20–50% in films 4, 7 (Figure 3). Moreover, the FWHM of the peak increased in all films (see the Table), which is opposite to the effect achieved during film annealing — decreasing FWHM and increasing reflection intensity resulting from strain relaxation [6]. δ estimated by parameter C increased in the films by 0.01–0.51 with its maximum $\delta = 0.62$. In film 1 deposited with lower filtration frequency than that for film 2, a single maximum with $2\theta = 38.17°$ was formed. In film 2, two maxima occurred at $2\theta = 37.98$ and $2\theta = 38.17°$ (Figure 4, *a* and *b*). If maxima (005) are believed to have been caused by the presence of regions with different oxygen content in film 2, then oxygen deficiency in the coherent scattering regions (CSR), where maxima are generated, will be $\delta \sim 0.7$ and 0.42 with mean value ~ 0.58. Decreasing peak intensity (005) in film 2 with ~ 1800 down to 900 arb. units after vacuum exposure (Figure 4, *a* and *b*) suggests decreasing number of CSR in each peak by a factor of two. Thus, in film 2, besides the loss of oxygen after vacuum exposure, two peaks occurred from CSR with different oxygen content, but with higher total FWHM resulting from the occurrence of crystallites with different oxygen content, i.e. different δ.

δ calculated from the angular position of the peak maximum (005) (Fig. 3) were 0.08 for film 3 and 0.17 for film 4, that should correspond to $T(R=0) = 87$ K in film 3 (as in film 7) and 84 K in film 4. Difference in peak shape (005) in films 3 and 4 after deposition was in the angular position of additional maxima at $2\theta = 38.38°$ in film 3 and $2\theta = 38.52°$ in film 4 (Figure 4, *c*). Oxygen content in CSRs that generate the maxima is higher than in CSRs that generate the peak with maximum intensity and δ is equal to 0 and 0.08 in films 3 and 4, respectively. On the HTSC phase diagram of these films, such δ could be located on opposite sides of maximum T_c, which resulted in equal $T(R=0) = 84$ K. After vacuum exposure of film 3, angular position of maxima with equal intensity at $2\theta = 38.295$ and $2\theta = 38.35°$ was $\delta = 0.24$ and 0.13 (Figure 4, *c*) with mean value $\delta = 0.18$ (see the Table). Thus, in film 3, mean value δ was unchanged, but occurrence of two diffraction peaks with similar intensity from CSRs with different oxygen content reduced the total diffraction intensity compared with diffraction peak of the film after deposition. In post vac film 4, two peaks were combined in a single peak with increased intensity at $2\theta = 38.34°$, i.e. film with an average oxygen content characterized by $\delta \sim 0.16$ was produced.

After vacuum exposure, oxygen deficiency δ (see the Table) in films 5 and 6 achieved ~ 0.6 (like in films 1 and 2), which was 0.38 and 0.25 as high as after deposition. Peak intensity in film 6 decreased negligibly and FWHM

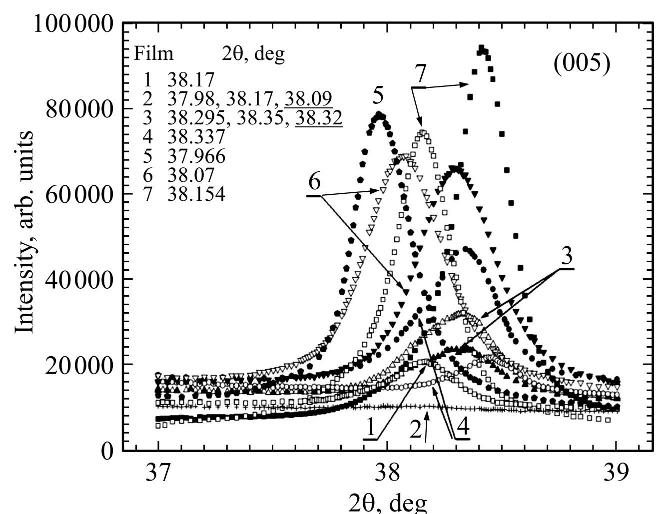

Figure 3. Diffraction peaks (005) of $YBa_2Cu_3O_{7-\delta}$ films with different $T(R=0)$: *7* — 87; *1, 2* — 85–85.8; *3, 4* — 84; *5, 6* — 77.4 K before (open symbols) and after 10^{-6} Pa 24 h vacuum exposure (filled symbols) of films. The Table lists the angular positions (mean value is underlined) of diffraction maxima of post vac films.

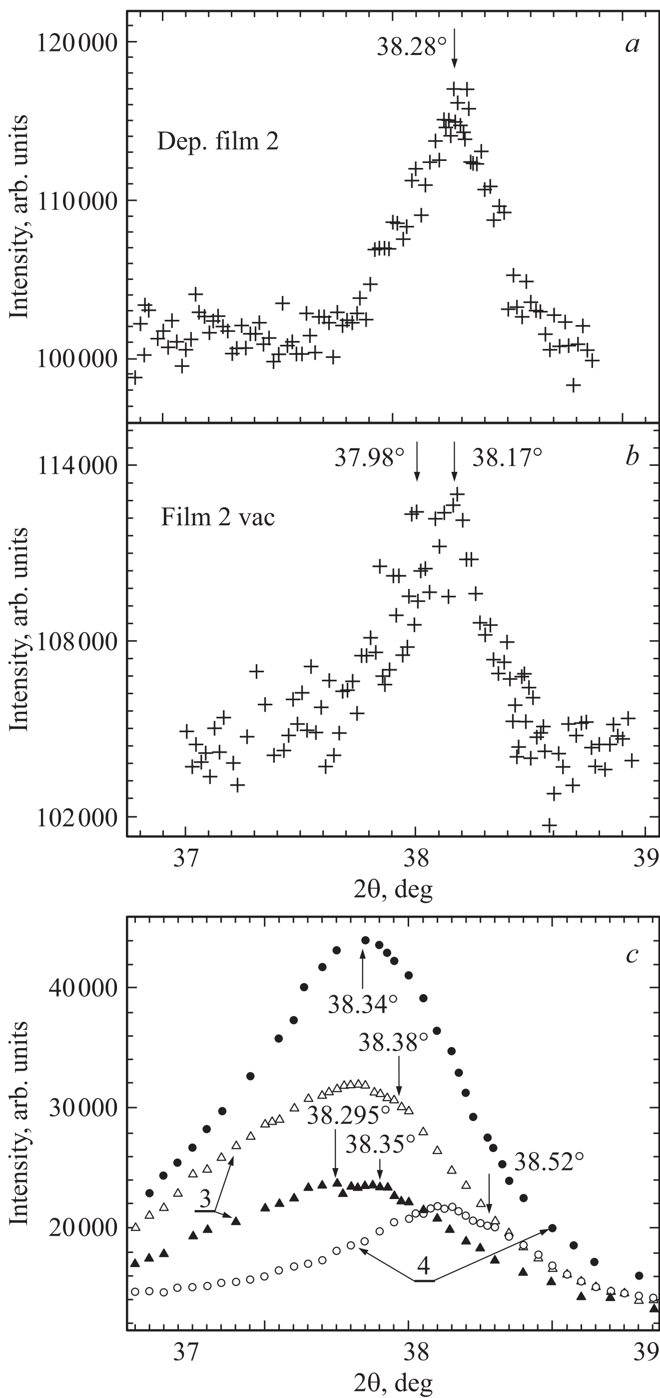

Figure 4. Zoom-in view of diffraction peaks (005): film *2* — before (*a*) and after (*b*) vacuum exposure; film *3* and *4* — before (open symbols) and after vacuum exposure (filled symbols) (*c*).

increased, which may be attributed to increasing strain on the crystalline structure as well as to increasing oxygen index scatter without occurrence of additional intensity diffraction peak. In film 7 produced without velocity filtration, intensity of reflection from CSR and oxygen deficiency δ increased. These changes may be caused by growth in the number of CSR during strain relaxation with loss of oxygen. Oxygen redistribution in CSR results in FWHM increase and reflection intensity decrease when additional maximum occurs (as in film 2), and in FWHM and reflection intensity increase when the main intensity peak merges with an additional one (as in film 4). Thus, increase in FWHM is related to strain and/or oxygen concentration scatter increase in the crystalline structure, while the diffraction peak intensity growth is related to the increase in the number of CSR.

3.3. Rocking curve analysis

Peak intensity on rocking curves recorded from films 1, 4, 5, 7 after deposition increased with decreasing filtration frequency, while a shape similar to (Figure 5,*a*) was relatively retained to some extent. Angular position of

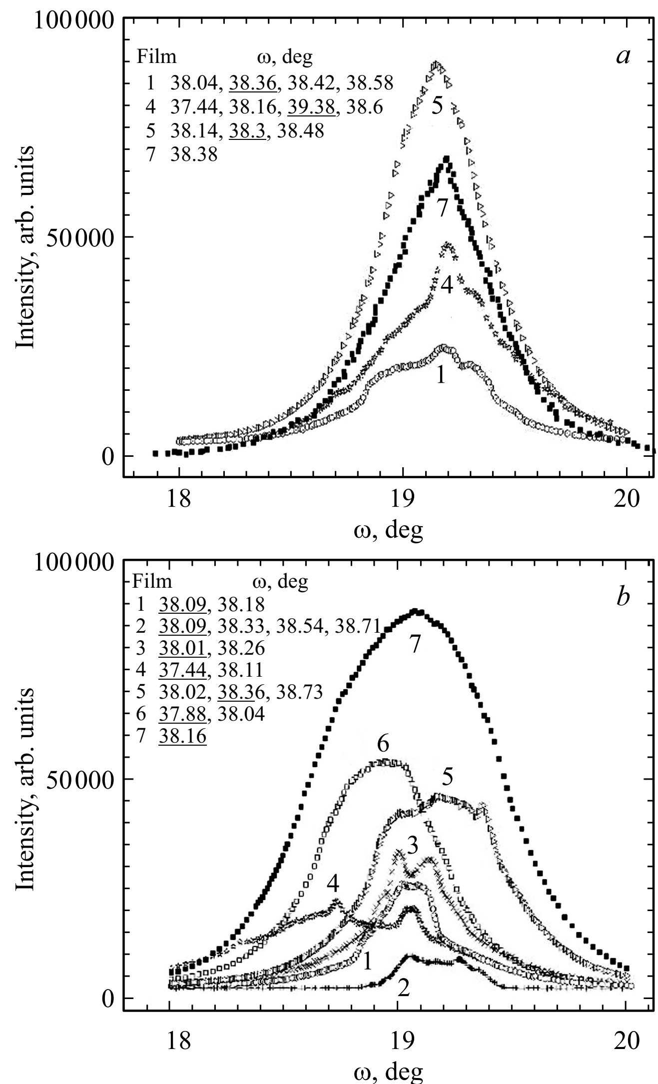

Figure 5. Peak (005) rocking curves of $YBa_2Cu_3O_{7-\delta}$ films with different $T(R=0)$: *1, 2* — 85.8; *3, 4* — 84; *5, 6* — 77.4; *7* — 87 K with constant 2θ for each film: before (*a*) and after (*b*) 10^{-6} Pa 24 h vacuum exposure. In the Tables, angular positions of peaks with maximum reflection intensity are underlined.

the main maximum was approximately maintained suggesting its consistent behavior. Movement of the maximum towards smaller angles proved the decrease in oxygen content. FWHM in films 1, 4, 5, 7 were equal to 0.9, 0.7, 0.58, 0.58° (see the Table), respectively, i.e. film 1 with the lowest intensity of diffraction peak (005) $\sim$ 26000 arb. units (Figure 5, a) had single-crystal grains with high deviation from [00l]. FWHM decrease in films with decreasing filtration frequency suggests better orientation to [00l] of crystallites with large intervals between deposition pulses. With lower deviation from [00l] (with smaller FWHM), films 5 and 7 were, in one case, formed by long-term deposition, and, in another case, were formed by deposition without filtering, i.e. from the flux in which fine particles were present together with large particles. In the same films 1, 4, 5, 7 exposed to vacuum, FWHM was 0.33, 0.64, 0.69, 0.7°, respectively. Reflection intensity (005) and FWHM on rocking curves depended both on the number and angular position of peaks. Thus, in film 1, two peaks with angular position difference 0.09° at 38.09 and 38.18° increased the reflection intensity and decreased FWHM from 0.9 to 0.33, and in film 4, the difference in extreme angular positions 0.7° of two peaks reduced the peak height and increased FWHM. Similarly, the difference in angular positions of peaks in film 5 $\sim$ 0.7° resulted in FWHM increase and height reduction. I. e large difference in extreme angular positions of additional peaks $\sim$ 0.7° (from individual groups of single-crystal grains) increased FWHM and angular deviation from [00l].

Therefore, angular position of maxima on the rocking curves characterizing orientation deviations of film single-crystal grains from crystallographic direction [00l] defined by the substrate structure and number of maxima affected the peak shape, height and FWHM. Changes in rocking curve shape, angular position and number of additional maxima (005) of films exposed to vacuum at 300 K are apparent and resulted from oxygen diffusion on the grain boundaries and structure defects caused by the film deposition conditions.

4. Discussion

Resistance R_{300} of films 1, 3, 6 and 7 after deposition (table in Figure 1) decreased with decreasing filtration frequency and increasing crystallite sizes equal to $\sim$ 2–10, 200–300, 500 and 1000 nm [13,15,16], respectively, in line with the knowledge about structure relaxation of films deposited at 720–740°C. The less dispersed structure from film 1 to film 7, the lower growth R_{300} was both before and after vacuum exposure (Table with R_{300} in Figure 1.), and this demonstrates high influence of grain boundaries on the hole transport in 'ab' plane. If R_{300} of 300 nm film 7 (Table with R_{300} in Figure 1.) is recalculated to 175 nm (R(film 7, $h = 175$ nm)$=$ R(film 7, $h = 300$ nm)$\times$300/175) both after deposition and vacuum exposure, then it will be $\sim$ 105 and 1966 Ω, respectively. Ratio of R_{300} of film 1 (206 Ω) to R_{300} recalculated to 175 nm of film 7 (105 Ω) after deposition is equal to $\sim$ 2, and ration of R_{300} of film 1 (26656 Ω) to R_{300} recalculated to 175 nm of film 7 (1966 Ω) after vacuum exposure is $\sim$ 14, while ratio of typical grain sizes remained unchanged $\sim$ 1000/5 $\sim$ 200, i.e. decreasing mean grain size increased resistance after deposition by a factor of 2 and by a factor of $\sim$ 14 after vacuum exposure. grain boundary resistance of films 1, 3, 6 and 7 after vacuum exposure can be believed to increase together with R_{300} by a factor of $\sim$ 130, 22, 25 and 18. Since the grain boundaries or CSR boundaries are surfaces with high diffusion and oxygen exchange with environment, then, when exposed to vacuum, they lose oxygen higher than the grain volume resulting in de-electrization of boundaries and film resistance growth before and after SC transition. Therefore, reduction of $T(R = 0.9R_{92})$ in films (see the Table) after vacuum exposure suggests that there is a difference in oxygen content inside crystallites and on crystallite boundaries. Oxygen-underdoped and optimally oxygen-doped thin films grown *in situ* at different oxygen pressures and deposition times from deposition temperature addressed by Riccardo Arpaia *et al.* [12] actually represented film exposure at different oxygen pressures (minimum pressure $1.5 \cdot 10^{-5}$ mbar) and allowed to detect the influence of oxygen content in films on $R(T)$ shape. Residual atmospheric (instead of oxygen) pressure in our vacuum chamber did not changed $R(T)$ shape: i.e. the slightly convex curve of film 7 and reduction of angle to the temperature axis showed high loss of oxygen, while the concave parabola in film 3 and convex parabola in films 1 and 6 characterized the impact of decreasing content on $R(T)/R_{300}$ shape. Thus, $R(T)/R_{300}$ shape (Figure 1 and 2) characterized not only δ and resistance of films before and after vacuum exposure, but also showed the loss of oxygen via the grain boundaries in vacuum at 300 K independent of the residual atmosphere composition.

Decreasing filtration frequency during deposition increased Bragg reflection intensities (005) representing CSR expansion up to the applicability boundary of the Selyakov–Scherrer relation $\sim$ 200 nm [13]. If the intensity of the highest diffraction maxima represents the fraction of particles that generate the maxima, then the ratio of Bragg reflections (005) from CSR film 7 (100000 arb. units) to reflection intensity (005) (1000–10000 arb. units) in films 1, 2 (Figure 3, 4) after deposition will estimate the number of 2–10 nm nanocrystals in the range from 90 to 99%, respectively, having good SC transition properties (see the Table) and $T(R = 0) = 85$–85.8 K. Ratio of reflection intensity (005) of films 3 and 6 to intensity (005) of film 7 (0.45 and 0.89) allows to estimate the number of nanocrystals in these films as 55% and 11%, respectively. However, if these reflection intensities decreased (Figure 3) in presence of additional peaks, then the provided estimate is understood as the maximum number of nanocrystals in films 2, 3. Since diffusion inside crystallites is a link that hampers the loss of oxygen by the film, then oxygen deficiency on the grain boundaries may be assumed as

higher than average. Achievement of $\delta = 0.7$ within the boundaries corresponds to the stability threshold of orthorhombic YBCO phase and will cause de-electrization of boundaries as well as near-boundary grain regions. With average $\delta = 0.58$ for film 2 (Figure 4, *b*, Table), deviation δ from 0.7 is 0.12 supporting the spatial variation δ found in thin YBCO film samples by Reiner *at al.* [8] by means of positron beam scanning that varied with a rms deviation up to 0.079 from the average value of one film in 'ab' plane.

Residual resistance after vacuum exposure of films attributed to the absence of SC phase on the intercrystallite boundaries, where $\delta \geq 0.7$, suggests reduction of oxygen content in films not only towards the free surface (along [00l]), but also in CuO_2 planes (along (00l)) between the grain boundaries and internals. Variation of $R(T)/R_{300}$ slope angles in the SC transition region after vacuum exposure (Detail in Figure 1) may be associated with oxygen redistribution inside the film both towards the free surface and CuO_2 planes. The latter assumption may be supported by $R(T)/R_{300}$ slope of SC transition in film 7 (Figure 2, Detail) retained after vacuum exposure of the film. In this case, lower oxygen content in the film volumes adjacent to the free and internal interfaces will increase the SC transition „entrance“ and „exit“ temperature range on curve $R(T)/R_{300}$, the loss of oxygen by the large grain internals will shift the SC transition on ~ 4 K to lower temperatures without considerable slope change (Figure 1, Table). In macroscopic YBCO single-crystals, evidence of superconducting regions with different, but close T_c were observed, i.e. regions with different δ [26]. In such case, disappearance of resistance was associated with formation of a cluster of regions with the same T_c, which covered the whole sample. The authors [26] did not suggest the origin of SC transition at different oxygen content in single-crystals, but it certainly depends on the oxygen content variation similar to that observed in crystallites of films 2, 3, 4 after deposition or vacuum exposure (Figure 4).

Additional maxima of reflection intensities (005) on diffraction patterns $\theta{-}2\theta$ in films 3 and 4 after deposition (Figure 4, *c*) correspond to approximate values δ calculated by their angular position 0.08 and 0.0, respectively. Since in films deposited at low pulse repetition rate (see the Table), additional diffraction maxima representing the regions with lower oxygen deficiency δ are not observed and the amount and average size of pyramids on their surface are higher, the main maximum may be suggested to be formed by diffraction from large pyramids [13,15,16]. Thus, films 3 and 4 with different oxygen content consist of pyramidal crystals of upper layer and lower layer where oxygen content is higher than in the upper layer. The difference in oxygen content in the upper and lower layers $\Delta\delta = 0.1$ coincides with the positron annihilation spectroscopy results with the variable energy positron beam in 230 nm films [7]. Films 3 and 4 with $\delta \sim 0.17$ after vacuum exposure could have been expected to show $T(R = 0)$ ~ 84 K, like after deposition (see the Table), however, broadening of diffraction peak (005) suggests an increase in the crystalline structure of mechanical stresses or changes in oxygen distribution. $R(T)/R_{300}$ slope in the SC transition region to the temperature axis in these films is lower than after deposition. Expansion of the SC transition region may be attributed to the presence of crystallites and/or clusters inside crystallites [25] with different oxygen content. In post vac film 4, the additional second maximum almost disappears being combined with the maximum peak and causing growth of maximum at $2\theta = 38.34^\circ$ (Figure 4, *c*). Peak intensity (005) shows that 60% of CSR (with respect to the film peak height 7) with average oxygen deficiency $\delta = 0.16$ is formed inside the film, i.e. oxygen content in the lower layer and pyramids became the same. When high loss of oxygen in post vac films 1, 2 with fine structure is assumed, then the maintenance of average oxygen amount $\delta \sim 0.16$ in films 3 and 4 may be attributed to the presence of faceted pyramids on their surface that consist of bars up to 10 nm in diameter [17] perpendicular to the substrate. Until the pyramids grow throughout the film thickness during the deposition time, they are single-crystals with low-angle boundaries between the bars inside them having lower permeability for oxygen atoms that the grain boundaries of films with dispersed structure. Such crystal reconstruction after deposition was observed in microdoped aluminium films [27] and bismuth films [28,29] where larger crystals with other orientation grew from the fine crystalline phase on the substrate. Minimum size of pyramids [13,16] on the surface after deposition was equal to $20{-}30$ nm. To cover 175 nm film surfaces completely, a layer of pyramids $25/175 \sim 15\%$ is required, which is lower than CSR fraction (45%) contained in film 3 and reduces the loss of oxygen.

Shape and angular position of maxima of the rocking curves in different post vac films did not show a common pattern, because they were generated from different initial structures [13]. However, films 1 and 2 with fine structure at $\omega = 19.45^\circ$ have one common maximum (Figure 5) that suggests some pattern of formation of larger crystals with perfect structure from nanocrystals obtained by deposition. FWHM of rocking curves in films 1, 4, 5, 7 was 0.9, 0.7, 0.58, 0.58° before vacuum exposure, and — 0.33, 0.64, 0.69, 0.7° after vacuum exposure, respectively, i.e. only in film 1, angular distribution of crystallite orientation decreased by a factor of ~ 2.5, while multidirectional changes within $\sim 15\%$ of values were observed in other films. However, shape, crystallite orientation and peak intensity variations on rocking curves are obvious after vacuum exposure and may result from oxygen diffusion at 300 K only. We suppose that, after vacuum exposure of films, mechanical strain occurs in them due to reduction of oxygen content resulting in crystallite orientation changes. Therefore, oxygen diffusion start temperature at 240°C in ~ 230 nm films [7,8] or oxygen diffusion start temperature at $\sim 180^\circ$C in 100 nm films [30] may be revised downwards to 300 K al least for post vac films.

5. Conclusion

These findings show that high mobility of oxygen atoms shall be taken into account to maintain the required properties of YBCO films not only in the process of their growth during deposition, but also for production and operation of 2D equipment and devices using vacuum technologies. This requirement is defined by increasing oxygen deficiency δ by ~ 0.5 in YBCO film structure with 2−10 nm crystallites, and by $\sim 0.25-0.35$ in films with crystallites larger than 500 nm within 24 hours at 300 K. The maximum rise of δ and resistance occur in films deposited from particles up to 40 nm at a filtration frequency of 28−33 Hz. A crystallite size of 2−10 nm corresponds to the increase in their surface area and facilitates oxygen diffusion over the surface, therefore, such films have dramatic reduction of oxygen index. Oxygen diffusion over the central single-crystalline part of grain is the channel that limits full loss of oxygen by the film. In this case, oxygen content on the boundaries is lower than the average value in the film and the boundary itself loses SC properties. The presence of grain boundaries on the working surfaces of 2D devices may result in degradation or loss of HTSC properties of the whole device in vacuum. Residual resistance resulting from loss of oxygen by boundaries proves that oxygen concentration gradient exists not only over the film thickness in direction [00l], but also in 'ab' plane in near-boundary grain regions, which degrades the film performance. Finally, changes in rocking curve shape, angular position and number of reflection maxima (005) after vacuum exposure at 300 K during 24 h could only occur as a result of oxygen diffusion over grain boundaries and other structure defects generated during film deposition. Decrease in the oxygen content in the crystalline structure should have occurred with formation of vacancies that have lower volume than the oxygen atom, which could be the cause of increase in strain and a driver of change in orientation of single-crystal grains and R_{300}. Analysis of the experimental X-ray diffraction results and transport properties of films obtained herein may allow to revise the oxygen diffusion start temperature in $\sim 100-230$ nm films from $\sim 180-240°$ C to 300 K al least for vacuum exposure of $YBa_2Cu_3O_{7-\delta}$ films.

Funding

This study was carried out under governmental job-order No. 075-01304-23-00.

Conflict of interest

The authors declare that they have no conflict of interest.

References

[1] N.E. Hussey. J. Phys.: Condens. Matter **20**, *12*, 123201 (2008).
[2] B. Dam, J. Rector, M.F. Chang, S. Kars, D.G. de Groot, R. Griessen. Appl. Phys. Lett. **65**, *12*, 1581 (1994).
[3] Pulsed Laser Deposition of Thin Films / Eds D.B. Chrisey G.K. Hubler. John Wiley & Sons Inc. N.Y. (1994).
[4] C. Gerger, D. Anslemetti, J.G. Bednorz, J. Mannhart, D.G. Schlom. Nature **350**, 279 (1991). https://doi.org/10.1038/350279a0
[5] B. Dam, J.H. Rector, J.M. Huijbregtse, R. Griessen. Physica C **305**, *1-2*, 1 (1998).
[6] J. Ye, K. Nakamura. Phys. Rev. B **48**, *10*, 7554 (1993).
[7] M. Reiner, T. Gigl, R. Jany, G. Hammerl, C. Hugenschmidt. Phys. Rev. B **97**, *14*, 144503 (2018).
[8] M. Reiner, T. Gigl, R. Jany, G. Hammerl, C. Hugenschmidt. Appl. Phys. Lett. **106**, 111910 (2015).
[9] T. Ito, K. Takenaka, S. Uchida. Phys. Rev. Lett. **70**, *25*, 3995 (1993).
[10] B. Wuyts, V.V. Moshchalkov, Y. Bruynseraede. Phys. Rev. B **53**, *14*, 9418 (1996).
[11] M.M. Abdelhadi, J.A. Jung. Phys. Rev. B **68**, *18*, 184515 (2003).
[12] R. Arpaia, E. Andersson, E. Trabaldo, Th. Bauch, F. Lombardi. Phys. Rev. Mater. **2**, 024804 (2018).
[13] A.I. Il'in, A.A. Ivanov, V.K. Egorov. FTT **63**, *9*, 1211 (2022). (in Russian).
[14] R. Arpaia, D. Golubev, R. Baghdadi, R. Ciancio, G. Drazic, P. Orgiani, D. Montemurro, T. Bauch, F. Lombardi. Phys. Rev. B **96**, *6*, 064525 (2017).
[15] A.I. Il'in, A.A. Ivanov. FTT **63**, *9*, 1209 (2021). (in Russian).
[16] A.I. Il'in, O.V. Trofimov, A.A. Ivanov. FTT **62**, *9*, 1555 (2020) (in Russian).
[17] A.I. Il'in, A.A. Ivanov, O.V. Trofimov, A.A. Firsov, A.V. Nikulov, A.V. Zotov. Mikroelektronika **48**, *147*, 2019 (2022). (in Russian).
[18] V.L. Gurtovoi, A.I. Il'in, A.V. Nikulov, V.A. Tulin. Low Temper. Phys. **36**, *10*, 974 (2010).
[19] A.A. Burlakov, V.L. Gurtovoy, A.I. Il'in, A.V. Nikulov, V.A. Tulin. Pis'ma v ZhETF **99**, *3*, 190 (2014). (in Russian).
[20] A.A. Burlakov, A.V. Chernykh, V.L. Gurtovoi, A.I. Il'in, G.M. Mikhailov, A.V. Nikulov, V.A. Tulin. Phys. Lett. A **381**, *30*, 2432 (2017).
[21] V.L.Gurtovoi, A.I. Il'in, A.V. Nikulov. Phys. Lett. A **384**, *26*, 126669 (2020).
[22] H.P. Klug, L.E. Alexander. X−Ray diffraction procedures. John Wiley & Sons, N.Y. (1974). 966 p.
[23] L.V. Azarov. X−Ray Diffraction. McGraw−Hill Book Company, N.Y. (1974). 664 p.
[24] B. Bucher, P. Steiner, J. Karpinski, E. Kaldis, P. Wachter. Phys. Rev. Lett. **70**, *13*, 2012 (1993).
[25] Y. Koike, Y. Iwabuchi, S. Hosoya, N. Kobayashi, T. Fukase. Physica C **159**, *1*, 105 (1989).
[26] R.V. Vovk, G.Ya. Khadzhai, Z.F. Nazyrov, S.N. Kamchatnaya, A. Feher, O.V. Dobrovolskiy. J. Mater. Sci. **29**, 6601 (2018).
[27] A.I. Il'in, E.E. Glikman, I.Yu. Borisenko, N.D. Zakharov, V.V. Starkov. Poverkhnost'. Fisika, khimiya, mekhanika **94**, 77 (1991). (in Russian)
[28] A.I. Il'in, A.V. Andreeva, B.N. Tolkunov. Mater. Sci. Forum. *207−209*, 625 (1996).
[29] A.I. Il'in, A.V. Andreeva. Fizika metallov i metallovedenie, **80**, *2*, 132 (1995). (in Russian).
[30] Yu.N. Drozdov, S.A. Pavlov, A.E. Parafin. Pis'ma v ZhTF,**55** (1998), 25 (2023) (in Russian).

Translated by Ego Translating